

# Real-time, continuous, fluorescence sensing in a freely-moving subject with an implanted hybrid VCSEL/CMOS biosensor

Thomas D. O'Sullivan,<sup>1,6</sup> Roxana T. Heitz,<sup>1,6</sup> Natesh Parashurama,<sup>2,6</sup> David B. Barkin,<sup>3</sup>  
Bruce A. Wooley,<sup>1</sup> Sanjiv S. Gambhir,<sup>2</sup> James S. Harris,<sup>1</sup> and Ofer Levi<sup>4,5,\*</sup>

<sup>1</sup> Department of Electrical Engineering, Stanford University, 420 Via Palou, Stanford, CA 94305-4075, USA

<sup>2</sup> Molecular Imaging Program at Stanford, Departments of Radiology and Bioengineering, Bio-X Program, Stanford University, Stanford, CA 94305, USA

<sup>3</sup> Texas Instruments, 2900 Semiconductor Driver, Santa Clara, CA 95052, USA

<sup>4</sup> Institute of Biomaterials and Biomedical Engineering, University of Toronto, 164 College Street, Toronto, Ontario, M5S 3G9, Canada

<sup>5</sup> The Edward S. Rogers Sr. Department of Electrical and Computer Engineering, University of Toronto, 10 King's College Road, Toronto, Ontario, M5S 3G4, Canada

<sup>6</sup> These authors contributed equally to this work  
[ofer.levi@utoronto.ca](mailto:ofer.levi@utoronto.ca)

**Abstract:** Performance improvements in instrumentation for optical imaging have contributed greatly to molecular imaging in living subjects. In order to advance molecular imaging in freely moving, untethered subjects, we designed a miniature vertical-cavity surface-emitting laser (VCSEL)-based biosensor measuring 1cm<sup>3</sup> and weighing 0.7g that accurately detects both fluorophore and tumor-targeted molecular probes in small animals. We integrated a critical enabling component, a complementary metal-oxide semiconductor (CMOS) read-out integrated circuit, which digitized the fluorescence signal to achieve autofluorescence-limited sensitivity. After surgical implantation of the lightweight sensor for two weeks, we obtained continuous and dynamic fluorophore measurements while the subject was un-anesthetized and mobile. The technology demonstrated here represents a critical step in the path toward untethered optical sensing using an integrated optoelectronic implant.

©2013 Optical Society of America

**OCIS codes:** (170.3890) Medical optics instrumentation; (130.6010) Sensors; (230.5160) Photodetectors; (130.5990) Semiconductors; (140.2020) Diode lasers.

## References and links

1. E. M. C. Hillman, C. B. Amoozegar, T. Wang, A. F. H. McCaslin, M. B. Bouchard, J. Mansfield, and R. M. Levenson, "In vivo optical imaging and dynamic contrast methods for biomedical research," *Philos Trans A Math Phys Eng Sci* **369**(1955), 4620–4643 (2011).
2. M. L. James and S. S. Gambhir, "A molecular imaging primer: modalities, imaging agents, and applications," *Physiol. Rev.* **92**(2), 897–965 (2012).
3. M. A. Pysz, S. S. Gambhir, and J. K. Willmann, "Molecular imaging: current status and emerging strategies," *Clin. Radiol.* **65**(7), 500–516 (2010).
4. M. Beiderman, T. Tam, A. Fish, G. A. Jullien, and O. Yadid-Pecht, "A Low-Light CMOS Contact Imager With an Emission Filter for Biosensing Applications," *IEEE Trans. Biomed. Circuits Sys.* **2**(3), 193–203 (2008).
5. B. A. Flusberg, A. Nimmerjahn, E. D. Cocker, E. A. Mukamel, R. P. Barretto, T. H. Ko, L. D. Burns, J. C. Jung, and M. J. Schnitzer, "High-speed, miniaturized fluorescence microscopy in freely moving mice," *Nat. Methods* **5**(11), 935–938 (2008).
6. T. O'Sullivan, E. A. Munro, N. Parashurama, C. Conca, S. S. Gambhir, J. S. Harris, and O. Levi, "Implantable semiconductor biosensor for continuous in vivo sensing of far-red fluorescent molecules," *Opt. Express* **18**(12), 12513–12525 (2010).
7. P. Valdastrì, E. Susilo, T. Förster, C. Strohhofer, A. Menciassi, and P. Dario, "Wireless implantable electronic platform for chronic fluorescent-based biosensors," *IEEE Trans. Biomed. Eng.* **58**(6), 1846–1854 (2011).

8. N. Parashurama, T. D. O'Sullivan, A. De La Zerda, P. El Kalassi, S. Cho, H. Liu, R. Teed, H. Levy, J. Rosenberg, Z. Cheng, O. Levi, J. S. Harris, and S. S. Gambhir, "Continuous sensing of tumor-targeted molecular probes with a vertical cavity surface emitting laser-based biosensor," *J. Biomed. Opt.* **17**(11), 117004 (2012).
9. K. Murari, R. Etienne-Cummings, G. Cauwenberghs, and N. Thakor, "An integrated imaging microscope for untethered cortical imaging in freely-moving animals," in *Engineering in Medicine and Biology Society (EMBC), 2010 Annual International Conference of the IEEE*, 2010), 5795–5798.
10. K. K. Ghosh, L. D. Burns, E. D. Cocker, A. Nimmerjahn, Y. Ziv, A. E. Gamal, and M. J. Schnitzer, "Miniaturized integration of a fluorescence microscope," *Nat. Methods* **8**(10), 871–878 (2011).
11. T. D. O'Sullivan, E. Munro, A. de la Zerda, N. Parashurama, R. Teed, Z. Walls, O. Levi, S. S. Gambhir, and J. J. S. Harris, "Implantable optical biosensor for in vivo molecular imaging," *Proc. SPIE Opt. Fiber and Sensors for Medical Diagnostics and Treatment Applications IX 717309* (2009).
12. M. Patterson, B. Wilson, and D. Wyman, "The propagation of optical radiation in tissue. II: Optical properties of tissues and resulting fluence distributions," *Lasers Med. Sci.* **6**(4), 379–390 (1991).
13. T. F. Massoud and S. S. Gambhir, "Molecular imaging in living subjects: seeing fundamental biological processes in a new light," *Genes Dev.* **17**(5), 545–580 (2003).
14. G. Vasilescu, *Electronic Noise and Interfering Signals: Principles and Applications* (Springer, Berlin, 2005).
15. R. T. Heitz, D. B. Barkin, T. D. O'Sullivan, N. Parashurama, S. S. Gambhir, and B. A. Wooley, "A low noise current readout architecture for fluorescence detection in living subjects," in *Solid-State Circuits Conference Digest of Technical Papers (ISSCC), 2011 IEEE International*, 2011), 308–310.
16. H. Ou and K. K. Chin, "Theory of gated multicycle integration (GMCI) for repetitive imaging of focal plane array," *IEEE Trans. Circuits Syst. II: Analog Digital Sig. Proc.* **50**(7), 378–383 (2003).
17. E. M. Sevick-Muraca and J. C. Rasmussen, "Molecular imaging with optics: primer and case for near-infrared fluorescence techniques in personalized medicine," *J. Biomed. Opt.* **13**(4), 041303 (2008).
18. S. P. Nichols, A. Koh, W. L. Storm, J. H. Shin, and M. H. Schoenfish, "Biocompatible materials for continuous glucose monitoring devices," *Chem. Rev.* **113**(4), 2528–2549 (2013).

## 1. Introduction

Optical imaging techniques are ubiquitous in biological research, most commonly for *in vitro* and preclinical studies, and are increasingly applied to clinical settings. Sources of optical contrast for imaging include *in vivo* fluorescence generated by reporter genes, endogenous fluorescence, and exogenous fluorescence from administered molecular probes or other contrast agents [1]. Optical signals can reveal underlying pathophysiology, quantify a molecular target, and localize specific cell populations while eliciting their temporal dynamics [2,3]. Fluorescence measurements can also complement label-free tissue evaluation, such as by detecting changes in optical absorption or scattering, which provide endogenous contrast useful for measuring tissue oxygenation as well as hemoglobin, water, lipid, and cytochrome concentrations.

Delineating normal from abnormal tissue requires the sensitive and quantitative detection of optical signals, but unfortunately, current approaches require bench-top systems employing bulky charge-coupled device (CCD) cameras or photomultiplier tubes and large-format illumination sources. These approaches, while non-invasive and highly sensitive, limit the ability to perform long-term, continuous measurements greater than several hours because of the inherent requirement to confine the animal subject to a light-tight box. We and others have developed miniature fluorescence-sensing systems that can be directly mounted on, or implanted in, an animal model [4–10] for continuous molecular monitoring in freely-moving subjects. Although potentially invasive, an implant also allows monitoring of deep tissues which may not be accessible with epi-illumination techniques. While this approach brings new challenges in the *in vivo* environment, it could be valuable for the early detection of disease, detecting disease (cancer) recurrence, monitoring disease progression and therapy, and even predicting disease occurrence (organ transplant rejection).

We have previously reported the fabrication and testing of a miniature, integrated semiconductor fluorescence sensor designed for the detection of Cyanine 5.5 (Cy5.5; GE Healthcare/Amersham)-based far-red / near-infrared (NIR) fluorescent probes [6,8,11]. The sensor incorporated three essential components of a fluorescence system, including a 670nm vertical-cavity surface-emitting laser (VCSEL) excitation source, a Gallium Arsenide (GaAs) p-i-n photodiode, and a fluorescence emission filter. Upon implantation of this sensor, we noted that the animal movement induced excessive electrical noise. The sensor's unamplified,

analog, sub-nanoamp current signal could not be distinguished from this noise. In this work, we integrated the sensor with a custom-developed, novel readout integrated circuit (ROIC) based on complementary metal-oxide semiconductor (CMOS) technology that amplifies and digitizes the raw current sensor signal, overcoming the noise limitations. The ROIC is directly interfaced with the fluorescence biosensor in a redesigned miniature hybrid package. In this work, we demonstrate the design, synthesis, and analysis of the fully functional hybrid biosensor. Furthermore, we demonstrate successful packaging, *in vivo* implantation with maintained functionality, and successful detection of fluorophore in a living subject. This approach should help pave the way for implantable, optical biosensors.

The paper is organized as follows: in Section 2 we briefly summarize (as some details have been published elsewhere) the design and fabrication of the implanted hybrid VCSEL/CMOS biosensor device, focusing on the efforts to make it suitable for implantation in preclinical models; Section 3 details the *in vitro* fluorescence sensitivity validation experiments using known concentrations of fluorescent dye; and in Section 4 we describe the implantation approach and present the real-time measurement of fluorescent dye in an awake, freely-moving nude mouse. Conclusions are presented in Section 5.

## 2. Implantable sensor design and fabrication

The implanted sensor, shown in Fig. 1(A) (inside) and 1(B) (in whole), consists of multiple VCSEL excitation sources, two GaAs photodiodes, and a CMOS ROIC mounted on a custom printed circuit board (PCB). This package is covered with a lid and a lens for collimating the excitation laser, and then completely coated in biocompatible epoxy to mitigate rejection upon implantation. The entire assembly is approximately 1cm<sup>3</sup> and weighs 0.7g, sufficiently lightweight for implanting in a small animal, and smaller than the dorsal skinfold window

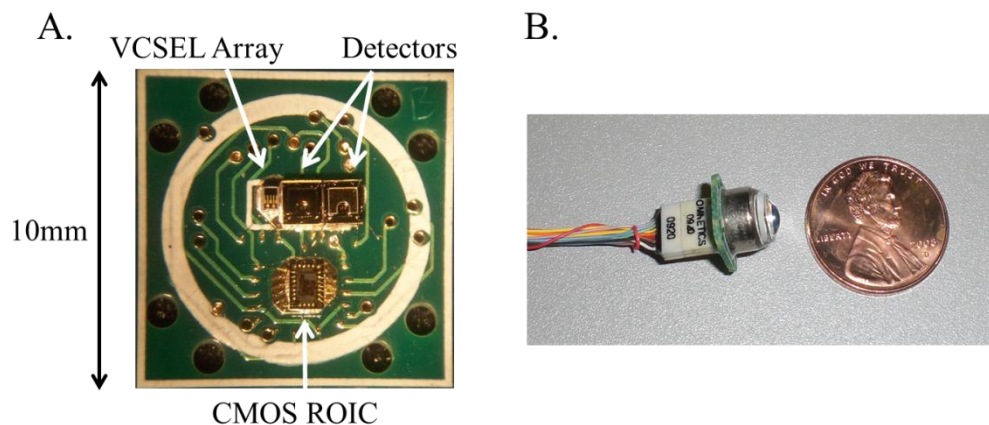


Fig. 1. (A) Implantable sensor custom PCB with bonded chips and (B) completed implantable sensor with cap, lens, and wire harness

chamber commonly used for *in vivo* imaging studies. During continuous sensing, a multi-conductor cable is connected to the PCB. This provides a biasing signal to the sensor and routes the measured, digitized signals from the animal subject to an external display.

### 2.1 Optoelectronic components

The optoelectronic components of the sensor module include an optical excitation source, a sensitive photodetector, and high quality fluorescence filters designed for particular fluorophores. We optimized our hybrid sensor for the detection of Cy5.5 fluorescent dye (Amersham/GE Healthcare), which can be conjugated to molecular binders (small molecules, macromolecules, protein fragments or proteins) to create molecular probes for *in vivo* studies

[8]. The excitation and emission spectra of Cy5.5 lies in the far-red to NIR spectral region, where tissue absorption is relatively minimal and the optical penetration depth can be large compared to other wavelengths [12]. Furthermore, tissue auto-fluorescence in this wavelength regime is low, and taken together, the signal to background ratio is increased compared to visible fluorescence imaging [13].

The optoelectronic components have been previously described in detail [6,8,11]. For completeness, we summarize those results here. The excitation source is an array of 670nm GaAs-based VCSELs provided by Vixar, Inc (Plymouth, MN) with laser linewidth less than 0.2nm full-width half-maximum (FWHM). We operate one laser which outputs up to 2mW optical power, matching the absorption peak of Cy5.5. The detector is a custom-fabricated large (0.75mm<sup>2</sup>) area GaAs p-i-n photodiode, optimized for low-noise, low dark current (<5pA/mm<sup>2</sup> at 0.1V) operation for maximum sensitivity. The fluorescence emission filter is the most critical element of the sensor for *in vivo* applications because a large fraction of tissue-backscattered excitation light is directed at the detector. The emission filter is designed for Cy5.5 emission (hq750/40, Chroma Technology Corp., Rockingham, VT) and is bonded directly above the GaAs detector. The 3mm thick filter is composed of RG absorbing glass and thin film coatings to provide more than 6 orders of magnitude optical blocking (OD 6) of excitation light at incident angles as high as 30 degrees and to transmit greater than 95% of emission light in a 40nm passband centered at 750nm. The combination of an absorption and interference-based optical filter is critical to achieving sufficient rejection in the small sensor format.

These optical components were separately evaluated and validated *in vitro* and *in vivo* in previous studies in a subcutaneous dye model, a phantom model, and a tumor model in which fluorescent molecular probe is injected systemically and accumulates in tumors [6,8]. Using these approaches, we achieved autofluorescence-limited sensitivity to subcutaneous fluorophore in a nude mouse. Cy5.5 concentrations as low as 5nM *in vitro* and 50nM *in vivo* were detected, with depth sensitivity estimated to be 1-2mm [6]. Furthermore, in those studies we detected kinetics of injected molecular probes, and a signal to background ratio of a molecular probe that targeted tumors was measured at approximately 2.4-3.6 to 1, similar to measurements in with a cooled CCD camera, and showing that the VCSEL biosensor functioned accurately.

## 2.2 CMOS readout circuit design

The CMOS ROIC is the enabling component of the implanted sensor. It amplifies and digitizes the detected photocurrent to enable real-time, implanted sensing. If the photocurrent were measured by a benchtop ammeter instead of being digitized on the sensor, the pico- to nano-amp photocurrent signals would be indistinguishable from the noise acquired by the small-gauge ammeter wires tethered to the moving animal. The sources of noise likely include the triboelectric effect (variations in charge due to rubbing of the conductor and dielectric insulator), piezoelectric effects [14], and inductive coupling to the cable.

The ROIC was designed to measure photocurrents in the range of 5pA to 15nA, with bandwidths up to 100Hz. In order to capture binding and accumulation kinetics of the fluorescent probe, as well as a wide range of possible tumor sizes and depths, we targeted a resolution of 5pA based on previous experiments.

The readout architecture (Fig. 2) is based on current integration using a capacitive transimpedance amplifier (CTIA), followed by analog-to-digital (A/D) conversion based on sigma-delta ( $\Sigma\Delta$ ) modulation [15]. The CTIA is used in order to meet the high sensitivity requirement, as it can provide a high signal-to-noise ratio (SNR) through noise averaging. The  $\Sigma\Delta$  modulator oversamples the output of the CTIA directly, while current integration takes place, and the digital filter at the output of the  $\Sigma\Delta$  modulator implements a line-fitting operation. This technique offers several improvements over the conventional approach of

measuring the CTIA signal at the end of the current integration period, including increased accuracy and the ability to extend the dynamic range (DR) using digital techniques.

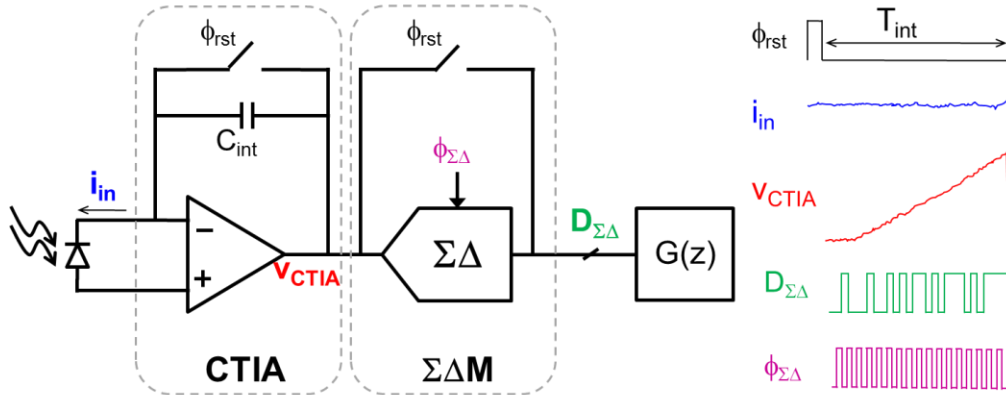


Fig. 2. Readout system architecture. The  $\Sigma\Delta$  modulator interfaces directly to the CTIA output, without the need for a sample-and-hold stage. Before each integration cycle, both the CTIA and the  $\Sigma\Delta$  modulator are reset. After the reset, the detector current accumulates on  $C_{int}$ , giving rise to a voltage ramp at the amplifier's output. This ramp is sampled by the  $\Sigma\Delta$  modulator  $M$  times during the integration period, and the output of the modulator is processed by a digital filter  $G(z)$  that implements a line-fitting operation similar to that described in [16]. Oversampling the ramp in this fashion reduces the readout noise by a factor of  $M/12$ .

The dynamic range of this current readout system can be extended by digital post-processing techniques, without the need for any additional circuit elements. If large photocurrents cause voltage saturation at the CTIA output, the line-fitting filter can be dynamically adjusted to only use the samples before saturation.

The chip operates from a 1.8V power supply and dissipates 1.4mW. It achieves a maximum SNR of 60.2dB and a DR of 60.2dB and 74.4dB before and after DR extension. The minimum resolvable current is 4pA and the maximum current is 21nA (with DR extension).

### 2.3 Assembly and packaging of hybrid sensor for implantation

Our objective was to design the smallest and lightest possible package for efficient implantation with enough leads to accommodate the devices. Therefore, the optoelectronic components and CMOS chip were chip-on-board mounted to a custom PCB. The semiconductor dies were attached with conductive epoxy (H20E, Epoxy Technology, Billerica, MA), and contacted with gold wire bonding. The right photodetector was wire bonded directly to the input of the ROIC and the left photodetector was connected to the external connector for signal comparison. We operated a single VCSEL source on the separate 1x5 VCSEL array. The PCB was designed to route the electrical signals from semiconductor dies to a miniature, multi-pin connector (A79010-001 18-pin connector, Omnetics, Minneapolis, MN) on the opposite side of the PCB. A standard transistor cap (TO-05) (4 mm high with 5 mm diameter aperture) was bonded to the PCB with biocompatible epoxy (301-2, Epoxy Technology, Billerica, MA) to protect the sensor components and support the lens. The lens was attached to the cap with ultraviolet cure epoxy for initial placement, and then the edge was strengthened with the biocompatible epoxy. The multi-pin connector was also reinforced by backfilling with epoxy. All locations where the copper vias on the PCB were exposed were coated with the insulating epoxy. Finally, several large holes were drilled in the corners of the PCB to allow the surgeon to suture the sensor into the animal subject. We rounded off the sharp edges from the PCB corners so as to not cause additional damage

underneath the skin. The entire implantable sensor (without the cable) weighs 0.7g and measures approximately 10 x 10 x 8mm.

### 3. *In vitro* validation

Because the previous VCSEL biosensor without the CMOS component was thoroughly validated in previous studies, we wanted to demonstrate that the VCSEL/CMOS hybrid biosensor operated equivalently *in vitro*. We measured the maximum sensitivity of the integrated CMOS and sensor chips *in vitro* by measuring serial dilutions of Cy5.5 in a benchtop system. The sensor components were mounted in an open cavity package and interfaced to a circuit which provided additional signal conditioning and diagnostics for the ROIC. A 7mm diameter clear-bottom plastic well (Stripwell 1 x 8, Corning Inc.) was suspended above the sensor. Cy5.5-NHS (GE Healthcare/Amersham) was hydrolyzed in phosphate buffer solution (PBS) to remove the reactive group and diluted at several concentrations in PBS.

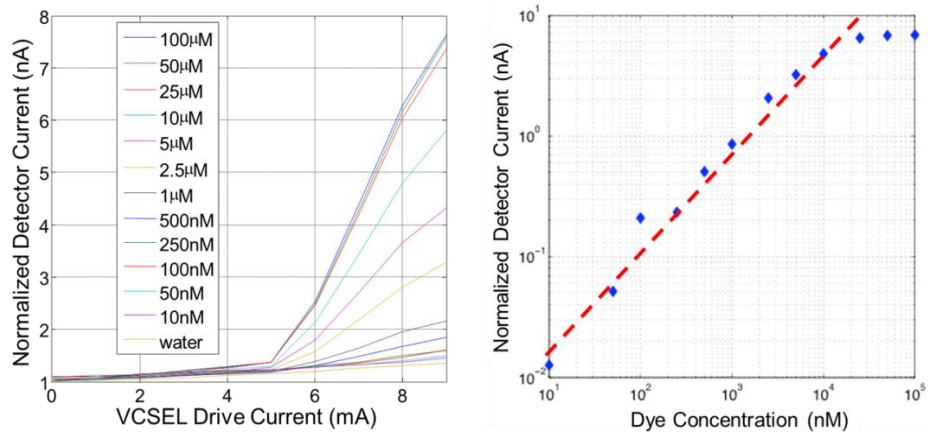


Fig. 3. Measurement of sensitivity using the on-package ROIC. Detected current increases linearly with Cy5.5 dye concentration until 25 $\mu$ M and are limited at the top by dye quenching effects.

Figure 3 shows the effects of varying dye concentration on detector current (normalized). As expected, the relationship between current and dye concentration is linear between 10nM and 25 $\mu$ M, and limited at the top by dye quenching effects and not by sensor performance. Lower concentrations may be detectable; 10nM was the lowest concentration tested. However, the signal would be indistinguishable from far-red autofluorescence *in vivo* at concentrations less than 50nM [17]. Our data is consistent with the sensitivity and magnitude of current that we have previously measured using the original VCSEL biosensor [6]. As a result, we are confident that this sensor is sensitive to at least 50nM subcutaneously localized Cy5.5 *in vivo*. Previously, we used low-frequency laser modulation with lock-in detection to achieve the best sensitivity. Now we show with the integrated VCSEL/CMOS sensor, we can operate the lasers in DC and achieve the same sensitivity. Since the ROIC bandwidth is sufficient to attempt lock-in detection, even better sensitivity might be possible, though this was not the focus of this study. Figure 3 also shows the importance of operating the laser above threshold to obtain the excitation intensity necessary to generate a detectable fluorescence signal.

### 4. Implantation and real-time sensing

An important issue for assessing *in vivo* sensing is the anatomical location of the biosensor in the mouse. The anatomical location should allow detection near the targeted tissue; securing

of the sensor to the underlying fascia and soft tissue should also be feasible. The mouse should be unable to access and annihilate the biosensor, and noise should be minimal. To this effect, we surgically investigated sensor locations using a prototype sensor in  $n = 2$  mice, to confirm a good mechanical stability of the sensor to the tissue following the procedure. After exploratory experiments, the biosensor was implanted subcutaneously in the midline for this initial demonstration, at the level of the 6th thoracic vertebrae on the back, and sutured to surrounding soft tissue. The details of the procedure are as follows. With the mouse in prone position under anesthesia, a 2cm vertical midline incision was made extending from the back of the neck to between the scapula. The subcutaneous tissues were divided to expose the deeper skeletal muscle layers of the back. A colored, labeled schematic of the VCSEL/CMOS biosensor is shown in Fig. 4(A). The biosensor was placed vertically into the surgically created cavity, with the cable-side on the outside, and aligned with the mouse spine. A colored, labeled schematic of the biosensor implanted into mouse tissue is shown in Fig. 4(B). We placed non-absorbable sutures in each corner of the biosensor. We anchored the skin firmly to the vertical portion of the device with a set of horizontal sutures (Fig. 4(B), Suture #1), and the remaining skin was then firmly approximated around the biosensor. Each internal suture anchored the sensor to the skin above (Fig. 4(B), Suture #2), or fascia/muscle below (Fig. 4B, Suture #3). Eventually, the lens directly faced the skeletal muscle, in order to sense tail vein injected Cy5.5 dye (Fig. 4(B)). The sensor was well secured in the mouse, and the mouse displayed normal feeding and ambulation with no evidence of distress. (Fig. 4(C), 4(D), and 4(E)).

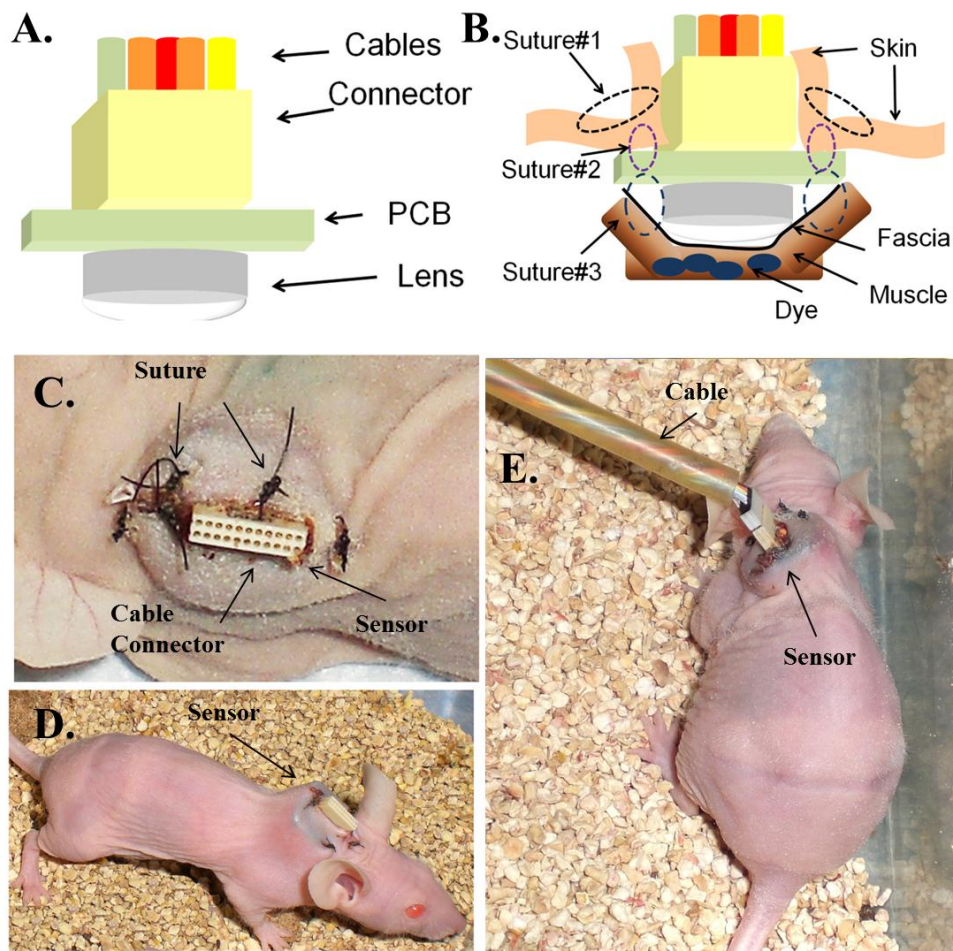


Fig. 4. Schematics (A, B) and photographs (C, D, E) of the miniature sensor implanted in a freely-moving nude mouse

A critical aspect of biosensing in a freely moving subject with the implanted biosensor is transmission of digitized information. To facilitate movement of the mouse, a multi-conductor cable was used to carry the electrical signal and bias voltages between the subject and instrumentation. The cable bundle was sheathed in latex tubing to prevent the animal from gnawing on the wires during sensing. Importantly, the cable bundle terminated at a commutator (SL18C, Plastics One Inc, Roanoke, VA) which allowed free rotation of the cables without losing electrical contact. Although the animal was able to move freely throughout its cage with the commutator, in some cases the 18 pin commutator was resistant to animal motion, so we occasionally rotated the commutator manually as needed to eliminate strain on the animal. In future versions, fewer leads will enable the use of a low mechanical resistance, brushless commutator to better facilitate animal movement. We evaluated implants in  $n = 2$  mice for greater than one week to verify sensor optical and electrical function, evaluate noise, and to monitor the mice for complications due to the surgery or implant.

After validating the surgical procedures and sensor performance, we performed a continuous measurement of fluorescence signal after dye injection in a freely moving mouse. 48 hours after implantation, we inserted a tail-vein catheter under anesthesia and performed baseline measurements for approximately 5 minutes (Fig. 5). Then during continuous

measurements we administered 50 $\mu$ L of 50 $\mu$ M Cy5.5 dye via the catheter. After injection, we flushed the catheter, removed the catheter and terminated the anesthesia. We continued sensing for more than 30 minutes while the mouse awoke and began to move freely. The acquired signal is shown in Fig. 5. An increase of 500pA up to 1.2nA increase can be seen about 15 minutes after injecting the dye, with the greatest increase occurring in the first 10 seconds. We also observed an additional spike in signal (at ~35 sec), due to the flushing of the remaining dye from the catheter with saline. For comparison, in previous studies, we observed a 50-85% increase in signal when 3 nmoles of fluorophore was injected [8]. In this study, upon injection of 2.5 nmoles, we saw an increase of 71%, within the range calculated previously. Furthermore, in the previous studies, we observed a similar rapid increase upon injection of fluorophore. These data suggested to us that the sensor was functioning in the mouse, in terms of both kinetics and absolute magnitude of the response.

Two weeks after implantation, there were no signs of infection, and the mouse continued to display normal feeding and ambulation with no loss of weight. At two weeks, we euthanized the animal in accordance with the approved animal protocol and the sensor was removed for inspection. Postmortem, we observed a small area of chronic scar tissue surrounding the implantation site and fibrous tissue attached to the sensor surfaces. This is an anticipated side effect of an implanted device, and if the layer thickness becomes significant compared to the 1-2mm depth of field of the device, this may become a problem. However, several approaches have been developed to mitigate sensor fouling which could also be applied here if necessary [18]. The source-detector separation could also be optimized to sense beyond the area of scar tissue.

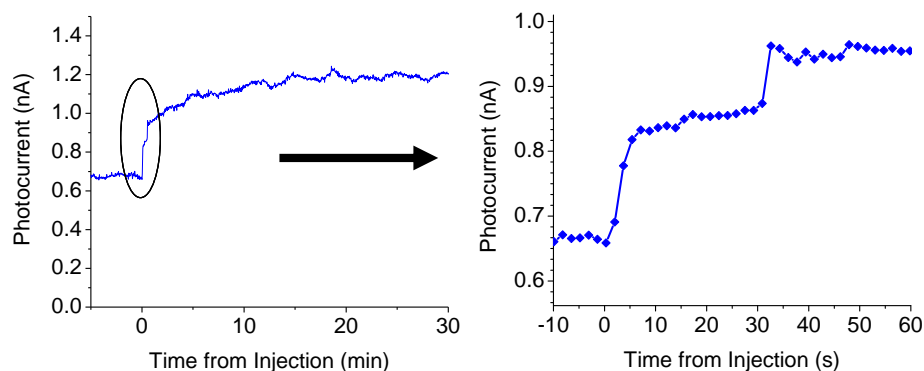


Fig. 5. Continuous measurement of implanted sensor signal in a mobile subject after tail vein injection of Cy5.5

## 5. Discussion and conclusions

We report for the first time (to the best of our knowledge), a laser sensor implant that makes continuous *in vivo* fluorescence measurements while the subject is awake and freely-moving. Unlike other approaches, all the sensing components are integrated on board so that the miniature implant can be completely wireless with the inclusion of a battery and a radio or data storage. Integration of a custom-designed, low-noise ROIC enabled real-time sensing of systemically administered fluorescent dye. Our previous studies have shown that the device is sensitive to molecular targets at pre-clinically relevant concentrations in an external sensing configuration [8].

The sensing volume of the tissue requires precise positioning and fixation of the sensor to sense specific targets. This is difficult to achieve in soft tissue, unless the target is expected to be large (> few mm) such as a tumor. We have evaluated mechanical stability, the function of the sensor, and its response to an injected dye, leading to continuous *in vivo* fluorescence

measurements. Due to the small target size, we believe the sensor may be appropriately suited for monitoring regional physiological parameters, such as hemodynamic changes, in which sensor positioning is not as critical. The sensor could also be affixed to hard structures, such as the skull for neurological studies. Relevant applications of this approach include monitoring of the progression and treatment of chronic diseases such as Alzheimer's, Parkinson's, or neurovascular diseases (stroke) for which molecular probes exist. Furthermore, the sensor components are scalable to allow optical sensing of different fluorophores (multiplexing) or multimodality sensing (measuring endogenous components, for example).

In conclusion, we have developed a fully-implantable, laser-based fluorescence sensor complete with optical and electrical read-out elements. This constitutes the first known laser-based implanted fluorescence detector. We have verified that the device operates while implanted in a live animal, and is sensitive enough to detect fluorophore at pre-clinically-relevant concentrations. Although this is an initial demonstration, we believe this technology platform has potential for the long term monitoring of disease progression and treatment.

### **Acknowledgments**

The authors are grateful for the helpful discussions and assistance during experiments with Dr. Robert Barretto as well as Mary Hibbs-Brenner and Klein Johnson from Vixar, Inc. for assistance in epitaxial growth. We acknowledge Chroma Technology Corp. for their generous donation of emission filter coatings. Funding for materials was provided through the Photonics Technology Access Program (PTAP) sponsored by NSF and DARPA-MTO and fabrication of devices was carried out in the Stanford Nanofabrication Facility (SNF). This work was supported in part through an Interdisciplinary Translational Research Program (ITRP) grant through the Stanford University Beckman Center for Molecular and Genetic Medicine (SSG & JSH) and from the National Cancer Institute ICMIC P50 CA114747 (SSG). It was also supported in part through the Natural Sciences and Engineering Research Council of Canada (NSERC) Discovery Grant RGPIN-355623-08, Collaborative Health Research Project Grant CPG-121050, and by the Networks of Centres of Excellence of Canada, Canadian Institute for Photonic Innovations (OL). TDO acknowledges graduate support from a National Defense Science and Engineering Graduate (NDSEG) fellowship, the U.S. Department of Homeland Security, and an SPIE scholarship. NP was supported in part by Stanford Dean's Fellowship, the Doris Duke Foundation, and Stanford NIBIB T32 Training grant EB009035.